

Ramifications of topology and thermal fluctuations in quasi-2D condensates

Arko Roy and D. Angom

Physical Research Laboratory, Navrangpura, Ahmedabad-380009, Gujarat, India

We explore the topological transformation of quasi-2D Bose-Einstein condensates of dilute atomic gases, and changes in the low-energy quasiparticles associated with the geometry of the confining potential. In particular, we show the density profile of the condensate and quantum fluctuation follow the transition from a multiply to a simply connected geometry of the confining potential. The thermal fluctuations, in contrast, remain multiply connected. The genesis of the key difference lies in the structure of the low-energy quasiparticles. For which we use the Hartree-Fock-Bogoliubov, and study the evolution of quasiparticles, the dipole or the Kohn mode in particular. We, then employ the Hartree-Fock-Bogoliubov theory with the Popov approximation to investigate the density and the momentum distribution of the thermal atoms.

PACS numbers: 03.75.Kk, 03.75.Hh, 67.85.Bc

I. INTRODUCTION

Toroidal or multiply connected condensates are splendid model systems to study Kibble-Zurek mechanism [1–3] in detail. Understanding of this mechanism in Bose-Einstein condensates (BECs), which explains spontaneous seeding of topological defects during phase-transitions, has attracted much attention. There has been several, both theoretical and experimental, recent works on this topic [4–7]. In this context, an investigation on the nature of quantum and thermal fluctuations in such systems is of importance, and can provide better insights to the physics of defect formation. Furthermore, toroidal BECs are significant as waveguides in atom interferometers [8], which are analogs of SQUIDs [9, 10].

The remarkable experimental realizations of toroidal condensates through a variety of sophisticated and novel techniques have opened up new possibilities to explore multiply connected BECs with finer control, and in better detail than ever before. To mention a few, toroidal condensates have been obtained with the use of harmonic potential in combination with a Gaussian potential [11], Laguerre-Gaussian beams [12–15], combination of an RF-dressed magnetic trap with an optical potential [16, 17], magnetic ring traps [18–21], time-averaged ring potentials [22, 23], coincident red and blue detuned laser beams [8], and employing digital micromirror devices [24]. For the present work, the realization consisting of a harmonic and Gaussian potential [11] is of importance as it offers the possibility of transforming harmonic (simply connected) to toroidal (multiply connected) confining potential by modifying the Gaussian potential. This is, in other words, equivalent to a pancake shaped BEC getting transformed to a toroidal one. The other, equally important, topics are the effects associated with the transition from multiply to simply connected BEC due to relative shift in the constituent trapping potentials. Here, the question “How do the fluctuations change as a multiply connected BEC is transformed to a simply connected one?” is a pertinent one. The answer to this question has profound experimental implications since, in experiments the trap centers never coincide. This is because of gravitational sagging, and deviations of the trapping potentials from perfect alignment.

In the present work, we use the Hartree-Fock-Bogoliubov

theory with Popov (HFB-Popov) approximation to gain insights on the quantum and thermal fluctuations as the separation between the trap centers increases. Starting from a perfectly aligned trapping potential to a misaligned configuration, our studies reveal that the multiply connected BEC gets transformed to a simply connected one. This is accompanied with the breaking of rotational symmetry of the system, and hardening of the quasiparticle excitations. Furthermore, we show that the quantum fluctuations have the same geometry as the BEC when the transformation from multiply to simply connected geometry occurs. But, the thermal fluctuations retains the multiply connected geometry. These are reflected in the momentum distribution of the quantum and thermal non-condensate densities. This indicates that the spontaneous seeding of topological defects can have different distributions depending on the geometry of the confining potential.

The paper is organized as follows: In Sec. II, we briefly explain the HFB-Popov formalism for interacting quasi-2D BEC and provide a description of how to compute the effective radial trapping frequencies associated with the change in the geometry of the confining potential. The results and discussions are given in Sec. III. The evolution of the quasiparticle excitation energy and amplitudes corresponding to the Kohn mode are presented in Sec. III A. The transition from multiply to simply connected geometry of the trapping potential brings about a change in the nature of quantum and thermal fluctuations and momentum distribution of the thermal atoms which are illustrated in Sec. III B, III C. The dispersion curves are then presented in Sec. III D. We, then, end with conclusions highlighting the key findings of the present work in Sec. IV.

II. HFB-POPOV APPROXIMATION IN QUASI-2D BEC

The second quantized form of the grand-canonical Hamiltonian describing an interacting quasi-2D BEC confined with trapping potential $V(x, y)$ is

$$\hat{H} = \iint dx dy \hat{\Psi}^\dagger(x, y, t) \left[-\frac{\hbar^2}{2m} \left(\frac{\partial^2}{\partial x^2} + \frac{\partial^2}{\partial y^2} \right) + V(x, y) - \mu + \frac{U}{2} \hat{\Psi}^\dagger(x, y, t) \hat{\Psi}(x, y, t) \right] \hat{\Psi}(x, y, t), \quad (1)$$

where, $\hat{\Psi}$ and μ are the Bose field operator of the single species BEC, and the chemical potential, respectively. Starting from a general 3D harmonic confining potential $V(x, y, z) = (1/2)m\omega_x^2(x^2 + \alpha^2 y^2 + \lambda^2 z^2)$, we obtain a rotationally symmetric quasi-2D system when the anisotropy parameters are $\alpha = \omega_y/\omega_x = 1$ and $\lambda = \omega_z/\omega_x \gg 1$. The excitations along z are then suppressed, and along this axis, the condensate remains in the ground state. Hence, we can integrate out the z dependence, and the confining potential is reduced to $V(x, y) = (1/2)m\omega_{\perp}^2(x^2 + y^2)$ and obtain the above Hamiltonian. With these considerations, the excitations and dynamics are limited to the xy -plane. Furthermore, the atoms repulsively interact with strength $U = 2a\sqrt{2\pi}\lambda$, with a as the s -wave scattering length, and m as the atomic mass. From the Hamiltonian, using the variational method with Bogoliubov approximation, we obtain a pair of coupled equations. These are the generalized Gross-Pitaevskii (GP) equation, and Bogoliubov-de Gennes equations. Together, the equations describe the equilibrium state of the condensate and non-condensed cloud of atoms in the confining potential at finite temperatures. For the present work, we use Hartree-Fock-Bogoliubov (HFB) theory to calculate the condensate and non-condensate density distributions. Further more, we use Popov approximation (HFB-Popov) to obtain gapless excitation spectra [25–29], and hence, maintain the Hugenholtz-Pines theorem [30].

In the HFB-Popov approach, the Bose field operator $\hat{\Psi}$ is a linear combination of the c -field or the condensate part represented by $\phi(x, y, t)$, and the non-condensate or the fluctuation part denoted by $\tilde{\psi}(x, y, t)$ [31]. That is, $\hat{\Psi} = \phi + \tilde{\psi}$ and the equation of motion of $\phi(x, y, t)$, the generalized GP equation, is

$$\hat{h}\phi + U[n_c + 2\tilde{n}]\phi = 0, \quad (2)$$

where, $\hat{h} = (-\hbar^2/2m)(\partial^2/\partial x^2 + \partial^2/\partial y^2) + V(x, y) - \mu$ represents the single-particle or the non-interacting part of the Hamiltonian. We obtain the generalized GP equation by reducing the three-field correlation term into a quadratic form in fluctuation operators based on Wick's theorem, and then, taking average to obtain the stationary state solution [31]. We define $n_c(x, y) \equiv |\phi(x, y)|^2$, $\tilde{n}(x, y) \equiv \langle \tilde{\psi}^\dagger(x, y, t)\tilde{\psi}(x, y, t) \rangle$, and $n(x, y) = n_c(x, y) + \tilde{n}(x, y)$ to be the local condensate, non-condensate, and total density, respectively. We use Bogoliubov transformation such that the fluctuations operator, in terms of the quasiparticle modes, are the following

$$\tilde{\psi} = \sum_j \left[u_j(x, y)\hat{\alpha}_j(x, y)e^{-iE_j t/\hbar} - v_j^*(x, y)\hat{\alpha}_j^\dagger(x, y)e^{iE_j t/\hbar} \right] \quad (3)$$

with $\hat{\alpha}_j$ ($\hat{\alpha}_j^\dagger$) as the quasiparticle annihilation (creation) operators which satisfy the usual Bose commutation relations, and the subscript j denotes the mode index. Here, u_j and v_j are the Bogoliubov quasiparticle amplitudes of the j th mode. From these definitions and considerations we arrive at the following pair of coupled Bogoliubov-de Gennes (BdG) equa-

tions

$$(\hat{h} + 2Un)u_j - U\phi^2 v_j = E_j u_j, \quad (4a)$$

$$-(\hat{h} + 2Un)v_j + U\phi^{*2}u_j = E_j v_j. \quad (4b)$$

We obtain the above equations by expressing the equation of motion of $\tilde{\psi}$ as that of $\hat{\Psi}$ with the subtraction of ϕ . To solve, the two equations are treated as matrix equation with eigenstates of the harmonic oscillator potential as the basis. The eigenvalues and eigenvectors of the matrix, obtained from diagonalizing the matrix, are then the quasiparticles or mode energies and amplitudes.

Once the quasiparticle energies and amplitudes are known, the thermal or non-condensate density \tilde{n} at temperature T is

$$\tilde{n} = \sum_j \{[|u_j|^2 + |v_j|^2]N_0(E_j) + |v_j|^2\}, \quad (5)$$

where $\langle \hat{\alpha}_j^\dagger \hat{\alpha}_j \rangle = (e^{\beta E_j} - 1)^{-1} \equiv N_0(E_j)$ with $\beta = 1/k_B T$, is the Bose factor of the j th quasiparticle state with energy E_j at temperature T . For $T \rightarrow 0$, the non-condensate density arises out of the quantum fluctuations when $N_0(E_j)$'s in Eq. (5) vanish. The non-condensate density is then reduced to $\tilde{n} = \sum_j |v_j|^2$. The essence of HFB-Popov theory is to obtain self-consistent solutions of the coupled equations Eq. (2) and Eq. (4).

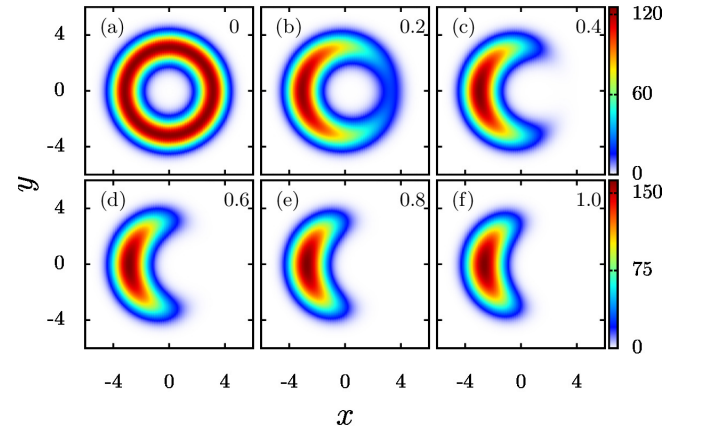


FIG. 1. (Color online) Plots of n_c at $T = 0$ for different values of Δ_x (shown at top right corner of each image). Shows the transformation of n_c from toroidal to bow-shaped structure. (a) For $\Delta_x = 0$, n_c assumes the form of a toroid which has a multiply-connected geometrical structure. (b) With $\Delta_x = 0.2$, the rotational symmetry of the condensate is broken, and (c) - (f) shows the simply-connected profiles of n_c when the trap centers are non-coincident. Here x, y , and Δ_x are measured in units of a_{osc} . In the plots n_c are in units of a_{osc}^{-2} .

A. Transition from Harmonic to toroidal potential

In the experiments with multiply connected BECs, toroidal in the present work, the confining potential could be a superposition of harmonic and Gaussian potentials with a common

center [11]. However, in practice, the trap centers do to coincide due to gravitational sagging or due to the fact that perfect alignment of optical and mechanical elements in experiments is improbable. Taking this into account, the net confining potential is

$$V_{\text{net}}(x, y) = V(x, y) + U_0 e^{-[(x-\Delta_x)^2 + \alpha^2 y^2]/2\sigma^2} \quad (6)$$

where, $V(x, y)$ is the harmonic potential described earlier, and second term is the Gaussian potential. In the latter, U_0 and σ are the amplitude and width, respectively. To simplify, we consider there is a relative separation Δ_x along x -axis between the minima of the harmonic potential $V(x, y)$ and maxima of the 2D-Gaussian potential. For the case of $U_0 = 0$ and $\Delta_x = 0$, when $\alpha = 1$, V_{net} is rotationally symmetric. For $U_0 \gg 0$ and $\Delta_x = 0$, V_{net} deviates from harmonic potential, and at larger values of U_0 the potential assumes the form of a doughnut or a toroid (multiply connected). The rotational symmetry is, however, broken for $\Delta_x \neq 0$. An intriguing possibility is to increase Δ_x , such that the two minima along the x axis are well separated in energies. As the Δ_x is increased, the geometry of the BEC is then transformed from toroidal to a bow-shaped structure as shown in Fig. 1. In the present work, we address the issues of how the relative shift affects the quasiparticles and the non-condensate densities. It must be mentioned here that, small values of Δ_x are important for realistic theoretical studies on finite temperature effects, and a continuous variation to large Δ_x offers a possibility to examine dynamics of topological defects, persistent currents, interplay of coupling between condensate and thermal clouds, and most importantly, evolution of mode energies and amplitudes. For the latter, the low energy excitations, the Kohn mode in particular, are of especial importance as quantum and thermal fluctuations have predominant contributions from these modes.

Although, we have considered toroidal potential as superposition of harmonic and Gaussian potentials, the other possibility is using Laguerre-Gaussian (LG_p^l) laser beams. These were first examined in theoretical works [32, 33], and eventually toroidal condensates of atomic ^{23}Na [12], and ^{87}Rb [13] have been experimentally achieved using LG_0^l beams [14]. It is worth mentioning here that in our earlier work [34], we demonstrated an alternative scheme of obtaining multiply connected BECs and its effects on the fluctuations. In the calculations, the spatial and temporal variables are scaled as x/a_{osc} , y/a_{osc} and $\omega_x t$ respectively, where $a_{\text{osc}} = \sqrt{\hbar/m\omega_x}$.

B. Effective radial trapping frequencies

One parameter which provides an insight on the condensate density distribution n_c with the variation in Δ_x is the effective radial trapping frequency ω_r of V_{net} . Consider the case of $\Delta_x = 0$, the V_{net} is then a rotationally symmetric Mexican hat potential, and ω_r about the minima of V_{net} is independent of the azimuthal angle ϕ . However, V_{net} breaks rotational symmetry when $\Delta_x \neq 0$ and the general form of the effective radial frequency is $\omega_r(\phi)$, it is a function of ϕ . For $\Delta_x > 0$, with the relative shift along the x -axis the

highest and lowest effective radial frequencies are $\omega_r(0)$ and $\omega_r(\pi)$, respectively. To compute these frequencies, let x_0 and x_π denote the two minima of V_{net} along the x -axis. This is a (a)symmetric double-well potential when ($\Delta_x > 0$) $\Delta_x = 0$, and with $\delta = x - x_{0,\pi}$, a Taylor series expansion about $x_{0,\pi}$ gives the effective harmonic oscillator potential around it as

$$V_{\text{eff}}(\delta) = \left\{ 1 + \frac{U_0}{\sigma^2} e^{-(x_{0,\pi}-\Delta_x)^2/2\sigma^2} \left[\frac{(x_{0,\pi}-\Delta_x)^2}{\sigma^2} - 1 \right] \right\} \delta^2, \quad (7)$$

and the effective radial frequencies are $\omega_r^2(0) = 1 + \frac{U_0}{\sigma^2} e^{-(x_0-\Delta_x)^2/2\sigma^2} \left[\frac{(x_0-\Delta_x)^2}{\sigma^2} - 1 \right]$, and $\omega_r^2(\pi) = 1 + \frac{U_0}{\sigma^2} e^{-(x_\pi-\Delta_x)^2/2\sigma^2} \left[\frac{(x_\pi-\Delta_x)^2}{\sigma^2} - 1 \right]$. The geometry of the condensate, and quasiparticle spectra depends on the relative values of these two frequencies. In addition, another important parameter is the energy difference $\Delta E = V_{\text{net}}(x_0, 0) - V_{\text{net}}(x_\pi, 0)$ between the minima along x -axis. Based on Thomas-Fermi approximation, where n_c is proportional to the confining potential, the condensate density profile is simply connected when $\mu < \Delta E$.

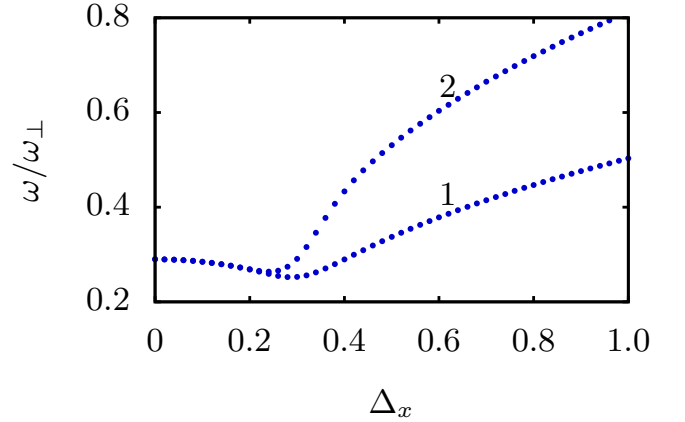


FIG. 2. (Color online) Evolution of Kohn mode energies as a function of Δ_x at $T = 0$. Shows the lifting of degeneracy of Kohn mode energy in the domain $0 \leq \Delta_x \leq 1$ as a result of topological deformation. The quasiparticle amplitudes corresponding to the energy branches '1' and '2' are structurally different. Here Δ_x is measured in units of a_{osc} .

C. Dispersion Relations

The dispersion relation of a physical system determines how it responds to external perturbations, in particular, those which can generate density variations at scales much smaller than the system size. For the present work, the transformation in the geometry of the external trapping potential from harmonic to toroidal, and the consequent transition of the BEC from multiply to simply connected topology affects the energy of the quasiparticle excitation. Hence, the dispersion relation is expected to change. For this, as the BEC is of finite size we compute the root mean square of the wavenumber k^{rms}

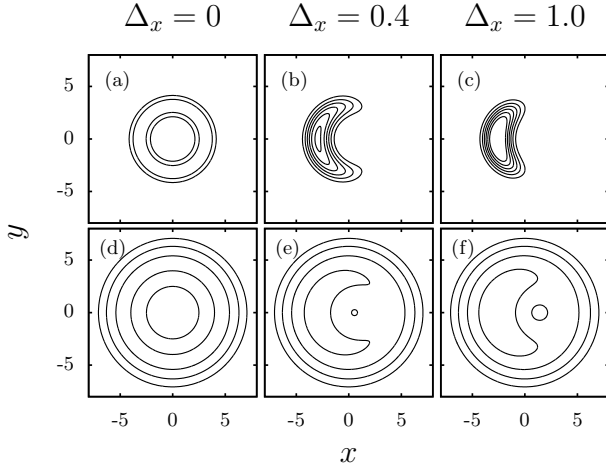


FIG. 3. (Color online) (a)-(c) The upper panel shows the contours of n_c , and (d)-(f) the lower panel shows the equipotential curves corresponding to three different values of Δ_x . Here x , y and Δ_x are measured in units of a_{osc} .

of each quasiparticle mode to define a discrete dispersion relation. Following Ref. [35], the k_j^{rms} of the j th quasiparticle is

$$k_j^{\text{rms}} = \left\{ \frac{\int d\mathbf{k} k^2 [|u_j(\mathbf{k})|^2 + |v_j(\mathbf{k})|^2]}{\int d\mathbf{k} [|u_j(\mathbf{k})|^2 + |v_j(\mathbf{k})|^2]} \right\}^{1/2}. \quad (8)$$

Here, it is to be noted that k_j^{rms} are in terms of the quasiparticle modes defined in the momentum space, and hence, it is essential to compute $u_j(\mathbf{k})$ and $v_j(\mathbf{k})$, the Fourier transform of the Bogoliubov quasiparticle amplitudes $u_j(x, y)$ and $v_j(x, y)$, respectively. Once we have k_j^{rms} for all the modes we obtain a dispersion curve, and we can then examine how the change in the condensate topology modifies the dispersion curve. In earlier works, dispersion curves have been obtained and examined for harmonically trapped binary BECs [36], binary BECs in optical lattices [37], and dipolar BECs [38, 39]. In this work we address how the topology of the BEC modifies the dispersion relation.

III. RESULTS AND DISCUSSIONS

To probe the effects of topological modification of the quasi-2D BEC from multiply to simply connected geometry, we solve the equations in HFB-Popov theory numerically. The results discussed are generic to BEC of any atoms with slight variations in the parameters, and for a detailed examination we consider the specific case of ^{23}Na BEC with $a = 53.3a_0$. Experimentally, toroidal condensates of ^{23}Na atoms have been achieved by combining a harmonic potential with a Gaussian potential [11]. The evolution of the quasiparticle modes is computed for $N_{\text{Na}} = 2 \times 10^3$ with $\lambda = 39.5$, $\omega_x = \omega_y = \omega_{\perp} = 2\pi \times 20.0$ Hz, and $U_0 = 15\hbar\omega_{\perp}$. At the outset when $U_0 = 15\hbar\omega_{\perp}$ and $\Delta_x = 0$, the density profile has rotational symmetry with $n_c(0, 0) \approx 0$ as shown in Fig. 1(a).

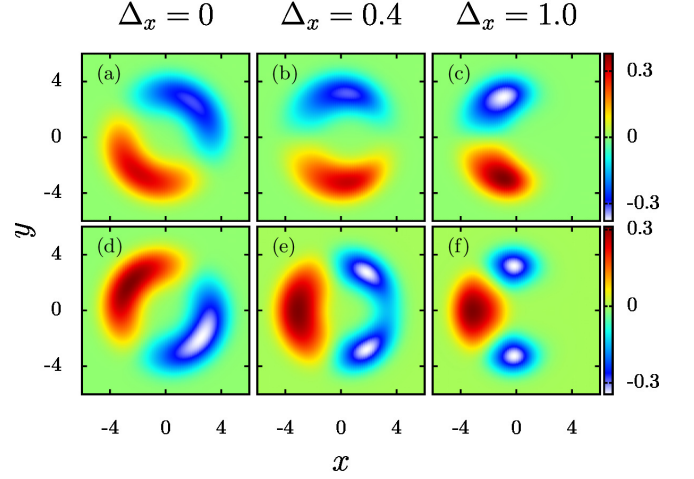


FIG. 4. (Color online) Evolution of quasiparticle amplitudes corresponding to the dipole or Kohn mode as Δ_x is varied from 0 to $1a_{\text{osc}}$. (a) - (c) Show the u_{Na} corresponding to the Kohn mode energies identified as ‘1’ in Fig. 2. (d) - (f) Show the u_{Na} corresponding to the Kohn mode energies identified as ‘2’ in Fig. 2. In the plots u and v are in units of a_{osc}^{-1} . Here x , y and Δ_x are measured in units of a_{osc} .

The condensate cloud assumes the form of a toroid. The low-lying excitation spectrum is characterized by the presence of doubly degenerate $m = 1$ modes, and among these, the most important ones are the Kohn modes with $\omega/\omega_{\perp} = 0.29$.

For studying mode evolutions, we do a series of computations using HFB-Popov approximation with increasing Δ_x to obtain the quasiparticle spectra and fluctuations. When $\Delta_x \neq 0$ the rotational symmetry of the potential and hence, the condensate cloud are broken. As Δ_x is increased, the profile of n_c is transformed from toroidal to bow-shaped geometry. This corresponds to a transition from multiply to simply connected topology, and the transition is shown in Fig. 1 with a set of selected values of Δ_x . The key point to note here is the modification of the excitation spectra and the structure of the Bogoliubov quasiparticle amplitudes. One of the most distinctive features is the evolution of the low-energy $m = 1$ modes. From these modes we select the one with lowest energy, the Kohn mode, and the evolution is as shown in Fig. 2 using HFB theory.

A. Kohn mode evolution

The Kohn modes, among the low-energy excitations, is one of the most important as it has leading contribution to quantum and thermal fluctuations. For this reason and as a case study, we examine its evolution in detail, however, the trends observed apply to other low-lying $m = 1$ modes as well. The Kohn mode is doubly degenerate when $\Delta_x = 0$, and as shown in Fig. 2, the degeneracy continues with decreasing energy in the domain $0 < \Delta_x \lesssim 0.22$. In this domain, the geometry of the condensate is multiply connected, but the density maxima is shifted radially outward. Thus, it increases the wavelength

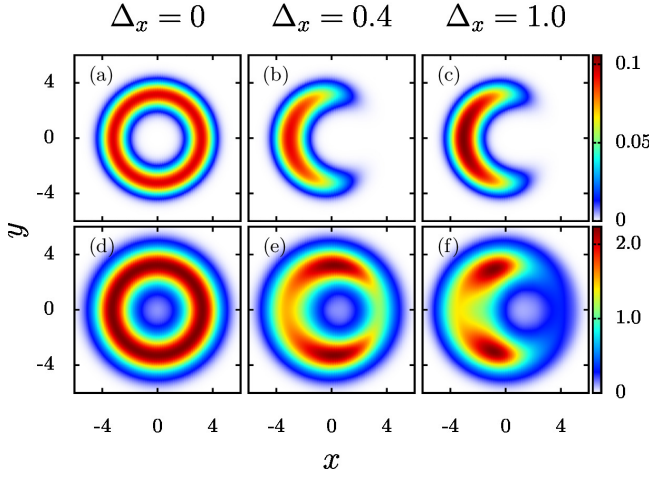


FIG. 5. (Color online) Condensate and non-condensate density profiles for different values of Δ_x . (a) - (c) plots of non-condensate density due to quantum fluctuations at $T = 0$, and (d) - (f) thermal density distribution at $T = 10$ nK for $\Delta_x = 0, 0.4, 1.0a_{\text{osc}}$, respectively. Here x, y , and Δ_x are measured in units of a_{osc} . In the plots \tilde{n} are in units of a_{osc}^{-2} .

of the excitations which lie along the toroidal axis, and explains the decrease in energy of the Kohn mode, and the other low-lying modes with $m = 1$. These observations are, as mentioned earlier, coupled to the form of the confining potential, and evident from the equipotential curves of V_{net} and density contours shown in Fig. 3(a) and (b).

At a critical value of Δ_x the toroidal condensate is transformed to a simply connected geometry. As a result, for $\Delta_x > 0.22$ the degeneracy of the Kohn modes is lifted, and the mode energy bifurcates into two branches marked as ‘1’ and ‘2’ in Fig. 2. In addition, the two modes harden, and there are discernible changes in the structure of the mode functions. As shown in Fig. 4(a), at $\Delta_x = 0$, the Kohn mode functions are $\pi/2$ rotation of each other and mutually orthogonal. However, with increase in Δ_x and after bifurcation, the mode function of the lower energy or the branch marked ‘1’ in Fig. 2 retains the dipole structure Fig. 4(a)-(c). But, the wave number increases, and hence, the two lobes gets smaller. For the other mode function with energy marked as ‘2’ in Fig. 2, one of the lobes begins to cleave for $\Delta_x > 0.22$, and as shown in Fig. 4(e) there are three distinct lobes at $\Delta_x \approx 0.4$. At higher values, say $\Delta_x = 1.0$, the three lobes are well separated, and it is effectively transformed into a mode which is neither $m = 1$ or $m = 2$, and its m may be considered as hybridization of 1 and 2. Thus, the increase in wave number, and transformation to a mode whose m is greater than unity accounts for the increase in the energies of the two modes.

B. Quantum and thermal fluctuations

Quantum fluctuations or zero temperature fluctuations, are intrinsic to any interacting quantum many-body system, and in the HFB-Popov approximation $|v|^2$ of the Bogoliubov quasi-

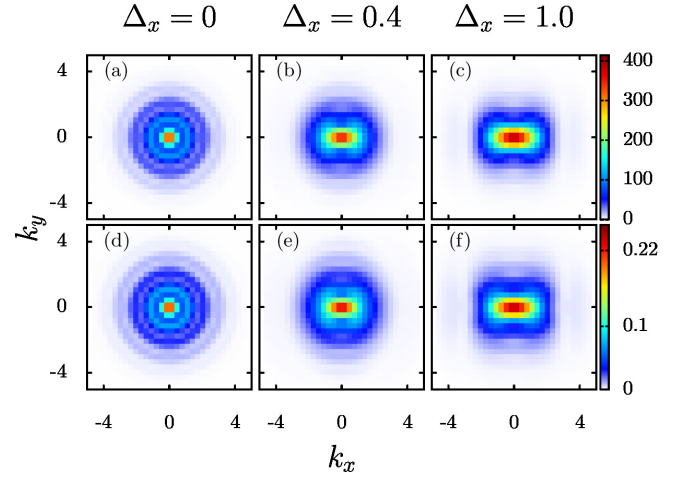


FIG. 6. Momentum distribution of the densities for different values of Δ_x at $T = 0$. (a)-(c) Show the momentum distribution corresponding to the condensate densities, (d)-(f) Show the momentum distribution corresponding to the non-condensate densities arising out of quantum fluctuations for $\Delta_x = 0, 0.4, 1.0a_{\text{osc}}$ respectively. Here k_x, k_y are measured in units of a_{osc}^{-1} .

particle amplitudes contribute to the quantum fluctuations. We find that with larger Δ_x , as the multiply connected condensate attains a simply connected geometry, there is a reduction in the total number of non-condensate atoms $\tilde{N} = \int \tilde{n}(x, y) dx dy$ with $\tilde{n}(x, y)$ as the non-condensate atom density. It is to be emphasized that $\tilde{n}(x, y)$ arising from quantum fluctuations coincides with the n_c for $\Delta_x \geq 0$, and specific examples are displayed in Figs. 5 (a)-(c).

For $T \neq 0$, both the quantum and thermal fluctuations contribute to \tilde{n} , however, the latter has a much larger contribution. When $\Delta_x = 0$, the condensate and the thermal clouds have similar density profiles, and possess overlapping maxima as shown in Fig. 5 (d). But, when $\Delta_x > 0$ the profiles evolve very differently with increase in Δ_x ; the profile of n_c is transformed to simply connected geometry, whereas \tilde{n} retains multiply connected structure as shown in Figs. 5 (e)-(f). In other words, there is a striking difference in the thermal component of \tilde{n} to that of the quantum fluctuations. This key difference is due to the thermal atoms filling up the region with depleted condensate density, and arises from the contributions to thermal fluctuations from quasiparticles with energies $E_j > \Delta E$. Where, ΔE as defined earlier is the energy difference between the two minima along the x -axis $V_{\text{net}}(x_0, 0) - V_{\text{net}}(x_\pi, 0)$.

C. Momentum distribution

To relate the condensate and non-condensate density profiles with the experimental observations based on time-of-flight imaging, it is important to have the momentum distribution of the atoms. For this reason, we compute the Fourier transform of the density profiles the k_x - k_y space. At $T = 0$, the momentum distribution of the condensate and the non-condensate densities have similar structures as shown in

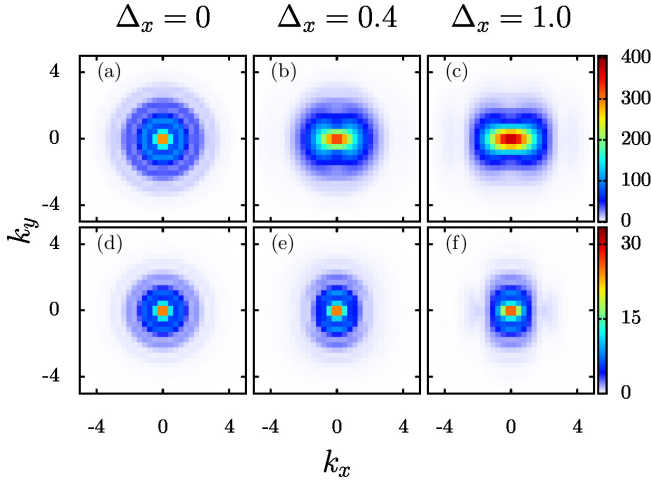


FIG. 7. Momentum distribution of the densities for different values of Δ_x at $T = 10\text{nK}$. (a)-(c) Show the momentum distribution corresponding to the condensate densities, (d)-(f) Show the momentum distribution corresponding to the non-condensate densities arising due to thermal atoms for $\Delta_x = 0, 0.4, 1.0a_{\text{osc}}$ respectively. Here k_x, k_y are measured in units of a_{osc}^{-1} .

Fig. 6 for different values of Δ_x . For $\Delta_x = 0$, the momentum distribution is rotationally symmetric in the k_x - k_y , but, when $\Delta_x \neq 0$ the rotational symmetry is broken. As Δ_x is increased the momentum distribution along x - and y -axis broaden and shrink, respectively. These are due to the decrease and increase in the spatial extent of the density distributions along x - and y -axis, respectively. Thus the change in the geometry of the trapping potential from multiply to simply connected is reflected in the momentum distribution.

In the case of $T \neq 0$, there is a marked difference between the momentum distributions of n_c and \tilde{n} . The momentum distribution of n_c at $T = 0$ and $T \neq 0$ are similar as evident from Fig. 7(a)-(c) for $\Delta_x \geq 0$. The thermal density \tilde{n} , on the other hand, has a very different momentum distribution compared to the quantum fluctuations. This is evident from the profile in k_x - k_y space shown in Fig. 7(d)-(f), and this emanates from the difference in the profile of \tilde{n} ; the contribution from the thermal fluctuations is multiply connected, whereas it is simply connected for quantum fluctuations. This difference in \tilde{n} was discussed earlier, and evident from the profiles in Fig. 5.

D. Dispersion Curves

To obtain the dispersion curves using Eq. (8) we compute k_j^{rms} of the j th quasiparticle mode for different Δ_x . For $\Delta_x = 0$, the azimuthal quantum number m is a good quantum number, and the modes with same m form branch like structures in the dispersion curves. The structure is discernible in the discrete dispersion curve in Fig. 8. However, for $\Delta_x > 0$ there is no discernible structure, and it is consistent with the absence of rotational symmetry in the system. More important, with the transition from multiply to simply connected geometry as Δ_x is changed from 0.0 to 0.4, for majority of the

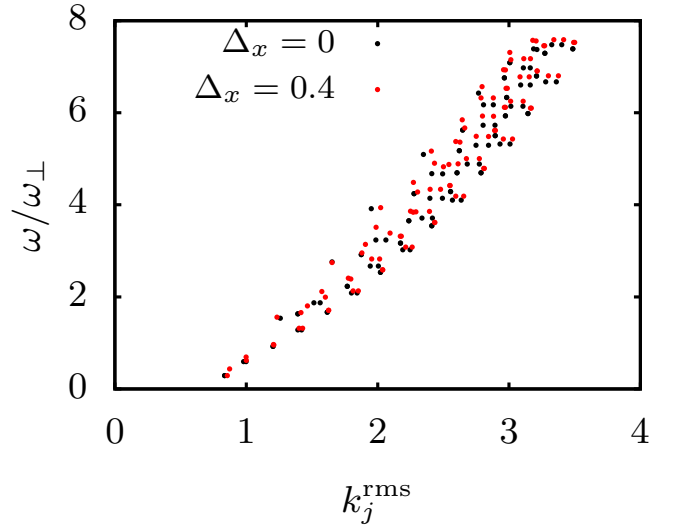


FIG. 8. The BdG quasiparticle dispersion curve for the transformation from multiply to symmetry-breaking simply connected topology. Here k_j^{rms} is in units of a_{osc}^{-1} .

modes k_j^{rms} remain unchanged, but the mode energies show an increase. This is a reflection of the mode hardening of the $m \neq 0$ modes discussed earlier. For a few, $m = 0$ and $n \neq 0$ or the radially excited modes in particular, the mode energies do not show any significant changes, but there is an increase in k_j^{rms} . The reason for this is the less number of low-energy modes with $n \neq 0$, so a change in $u_j(\mathbf{k})$ and $v_j(\mathbf{k})$ due to increase in Δ_x has prominent effects on k_j^{rms} .

IV. CONCLUSIONS

The present studies reveal dramatic modification of the condensate, and thermal density profiles when the harmonic and Gaussian confining potentials in a toroidal trap configuration have non-coincident centers. More importantly, larger separation of the trap centers transforms the topology of the system. Starting from a multiply connected density profile, as the separation between the trap centers is increased, above a critical value a simply connected condensate profile emerges as the ground state configuration. An important observation associated with this transition is the lifting of the degeneracy of the low-lying quasi particles, and subsequent increase in the mode energies. This is due to the modification of the radial trapping frequencies of the effective external confining potential.

Our finite temperature results using HFB-Popov approximation demonstrate a contrasting trends in the quantum and thermal fluctuations as a function of the separation of trap centers. The quantum fluctuations resembles the condensate density distribution, and undergoes a transformation from multiply connected to simply connected geometry. Thermal fluctuations, on the other hand, remains multiply connected. This leads to discernible differences in the TOF density evolutions, which could be detected in experiments.

ACKNOWLEDGMENTS

We thank K. Suthar, S. Bandyopadhyay and R. Bai for useful discussions. The results presented in the paper are based

on the computations using Vikram-100, the 100TFLOP HPC Cluster at Physical Research Laboratory, Ahmedabad, India.

-
- [1] T. W. B. Kibble, *J. Phys. A* **9**, 1387 (1976).
 - [2] W. H. Zurek, *Nature (London)* **317**, 505 (1985).
 - [3] W. Zurek, *Phys. Rep.* **276**, 177 (1996).
 - [4] C. N. Weiler, T. W. Neely, D. R. Scherer, A. S. Bradley, M. J. Davis, and B. P. Anderson, *Nature* **455**, 948 (2008).
 - [5] A. Das, J. Sabbatini, and W. H. Zurek, *Scientific Reports* **2**, 352 (2012).
 - [6] G. Lamporesi, S. Donadello, S. Serafini, F. Dalfovo, and G. Ferrari, *Nat. Phys.* **9**, 656 (2013).
 - [7] S.-W. Su, S.-C. Gou, A. Bradley, O. Fialko, and J. Brand, *Phys. Rev. Lett.* **110**, 215302 (2013).
 - [8] G. E. Marti, R. Olf, and D. M. Stamper-Kurn, *Phys. Rev. A* **91**, 013602 (2015).
 - [9] C. Ryu, P. W. Blackburn, A. A. Blinova, and M. G. Boshier, *Phys. Rev. Lett.* **111**, 205301 (2013).
 - [10] R. Mathew, A. Kumar, S. Eckel, F. Jendrzejewski, G. K. Campbell, M. Edwards, and E. Tiesinga, *Phys. Rev. A* **92**, 033602 (2015).
 - [11] C. Ryu, M. F. Andersen, P. Cladé, V. Natarajan, K. Helmerson, and W. D. Phillips, *Phys. Rev. Lett.* **99**, 260401 (2007).
 - [12] A. Ramanathan, K. C. Wright, S. R. Muniz, M. Zelan, W. T. Hill, C. J. Lobb, K. Helmerson, W. D. Phillips, and G. K. Campbell, *Phys. Rev. Lett.* **106**, 130401 (2011).
 - [13] S. Moulder, S. Beattie, R. P. Smith, N. Tammuz, and Z. Hadzibabic, *Phys. Rev. A* **86**, 013629 (2012).
 - [14] J. E. Curtis and D. G. Grier, *Phys. Rev. Lett.* **90**, 133901 (2003).
 - [15] S. Beattie, S. Moulder, R. J. Fletcher, and Z. Hadzibabic, *Phys. Rev. Lett.* **110**, 025301 (2013).
 - [16] W. H. Heathcote, E. Nugent, B. T. Sheard, and C. J. Foot, *New J. Phys.* **10**, 043012 (2008).
 - [17] O. Morizot, Y. Colombe, V. Lorent, H. Perrin, and B. M. Garraway, *Phys. Rev. A* **74**, 023617 (2006).
 - [18] J. A. Sauer, M. D. Barrett, and M. S. Chapman, *Phys. Rev. Lett.* **87**, 270401 (2001).
 - [19] S. Gupta, K. W. Murch, K. L. Moore, T. P. Purdy, and D. M. Stamper-Kurn, *Phys. Rev. Lett.* **95**, 143201 (2005).
 - [20] A. S. Arnold, C. S. Garvie, and E. Riis, *Phys. Rev. A* **73**, 041606 (2006).
 - [21] B. E. Sherlock, M. Gildemeister, E. Owen, E. Nugent, and C. J. Foot, *Phys. Rev. A* **83**, 043408 (2011).
 - [22] K. Henderson, C. Ryu, C. MacCormick, and M. G. Boshier, *New J. Phys.* **11**, 043030 (2009).
 - [23] T. A. Bell, J. A. P. Glidden, L. Humbert, M. W. J. Bromley, S. A. Haine, M. J. Davis, T. W. Neely, M. A. Baker, and H. Rubinsztein-Dunlop, *New J. Phys.* **18**, 035003 (2016).
 - [24] A. Kumar, N. Anderson, W. D. Phillips, S. Eckel, G. K. Campbell, and S. Stringari, *New J. Phys.* **18**, 025001 (2016).
 - [25] C. Gies, B. P. van Zyl, S. A. Morgan, and D. A. W. Hutchinson, *Phys. Rev. A* **69**, 023616 (2004).
 - [26] C. Gies and D. A. W. Hutchinson, *Phys. Rev. A* **70**, 043606 (2004).
 - [27] A. Roy, S. Gautam, and D. Angom, *Phys. Rev. A* **89**, 013617 (2014).
 - [28] A. Roy and D. Angom, *Phys. Rev. A* **90**, 023612 (2014).
 - [29] A. Roy and D. Angom, *Phys. Rev. A* **92**, 011601(R) (2015).
 - [30] N. M. Hugenholtz and D. Pines, *Phys. Rev.* **116**, 489 (1959).
 - [31] A. Griffin, *Phys. Rev. B* **53**, 9341 (1996).
 - [32] E. M. Wright, J. Arlt, and K. Dholakia, *Phys. Rev. A* **63**, 013608 (2000).
 - [33] J. Courtial, K. Dholakia, L. Allen, and M. J. Padgett, *Phys. Rev. A* **56**, 4193 (1997).
 - [34] A. Roy and D. Angom, arXiv:1511.08655 [cond-mat.quant-gas] (2015).
 - [35] R. M. Wilson, S. Ronen, and J. L. Bohn, *Phys. Rev. Lett.* **104**, 094501 (2010).
 - [36] C. Ticknor, *Phys. Rev. A* **89**, 053601 (2014).
 - [37] K. Suthar and D. Angom, arXiv:1603.02455 [cond-mat.quant-gas] (2016).
 - [38] P. B. Blakie, D. Baillie, and R. N. Bisset, *Phys. Rev. A* **88**, 013638 (2013).
 - [39] R. N. Bisset, D. Baillie, and P. B. Blakie, *Phys. Rev. A* **88**, 043606 (2013).